Neurobiology of Aging 84 (2019) 208–216

Contents lists available at ScienceDirect

Neurobiology of Aging

journal homepage: www.elsevier.com/locate/neuaging

Age dependency of mGluR5 availability in 5xFAD mice measured by PET

Minkyung Lee [a,1], Hae-June Lee [b,1], Ye Ji Jeong [b], Se Jong Oh [c], Kyung Jun Kang [c], Sang Jin Han [c], Kyung Rok Nam [c], Yong Jin Lee [c], Kyo Chul Lee [c], Young Hoon Ryu [d], In Young Hyun [a], Jae Yong Choi [c,*]

[a] Department of Nuclear Medicine, Inha University Hospital, Inha University, Incheon, South Korea
[b] Division of Radiation Effects, Korea Institute of Radiological and Medical Sciences, Seoul, South Korea
[c] Division of Applied RI, Korea Institute of Radiological and Medical Sciences, Seoul, South Korea
[d] Department of Nuclear Medicine, Gangnam Severance Hospital, Yonsei University College of Medicine, Seoul, South Korea

ARTICLE INFO

Article history:
Received 6 December 2018
Received in revised form 29 July 2019
Accepted 6 August 2019
Available online 9 August 2019

Keywords:
Alzheimer's disease
5xFAD
Beta-amyloid
PET
MRS

ABSTRACT

The major pathologies of Alzheimer's disease (AD) are amyloid plaques and hyperphosphorylated tau. The deposition of amyloid plaques leads to synaptic dysfunction, neuronal cell death, and cognitive impairment. Among the neurotransmitters, glutamate is the most abundant in the mammalian brain and plays an important role in synaptic plasticity. With respect to synaptic transmission, metabotropic glutamate receptor 5 (mGluR5) is highly affected by amyloid pathology. However, the neuropathologic changes in the protein expression of mGluR5 in AD remain unclear. Therefore, to elucidate the alteration in mGluR5 expression with the progression of AD, we performed serial behavioral tests, longitudinal imaging studies, and histopathological immunoassay for both 5xFAD (n = 14) mice and age-matched wild-type mice (n = 14). The 5xFAD mice started showing severe hyperactivity and memory impairment from 7 months of age. In addition, mGluR5 positron emission tomography revealed that while the binding values in the wild-type mice were similar over time, those in 5xFAD mice fluctuated from 5 months of age. Furthermore, the 5xFAD mice presented a 35% decrease in the binding values of their cortical and subcortical areas at 9 months of age compared with those at 3 months of age. Magnetic resonance spectroscopy and histopathological studies showed similar changes. In conclusion, mGluR5 availability changes with age, and mGluR5 positron emission tomography could successfully detect this synaptic change in the 5xFAD mice.

1. Introduction

Alzheimer's disease (AD) is the most common etiology of dementia, and its primary clinical characteristic features include gradual decline in multiple cognitive functions, as well as manifestation of noncognitive neuropsychiatric symptoms (Larson et al., 1992). The neuropathological hallmarks of AD are senile plaques, which are extracellular deposits of amyloid β (Aβ), and the intracellular accumulation of neurofibrillary tangles, which contain hyperphosphorylated tau protein, in the brain (Alzheimer et al., 1995). These proteinopathies cause neuronal cell death in the regions of the cortex and hippocampus that affect memory formation. They also affect the cortical regions responsible for language, reasoning, and social behavior (Grothe et al., 2017; Reilly et al., 2003), as the disease progresses. Although many researchers attempted to uncover the pathophysiology underlying AD, major issues regarding synaptic homeostasis are yet to be fully understood.

Numerous studies reported that amyloid β oligomer (Aβo) induces synaptic damage and consequent disturbance in neurotransmission systems (i.e., serotonin, noradrenaline, acetylcholine, dopamine, and glutamate) in patients with AD (Francis et al., 2010; Reinikainen et al., 1990; Xu et al., 2012). Considering that synapses are the fundamental units of information transfer, the prevention and treatment of AD may require a detailed understanding of the mechanism that causes disturbances in synaptic neurotransmission. Glutamate is the most abundant neurotransmitter, and it plays a crucial role in neuronal plasticity, which underlies learning and memory formation (Allen and Barres, 2005; Fields and Stevens-

* Corresponding author at: Division of Applied RI, Korea Institute of Radiological and Medical Sciences, Seoul, South Korea. Tel.: +82 2 970 1639; fax: +82 2 970 1987.
E-mail address: smhany@kirams.re.kr (J.Y. Choi).
[1] Both authors contributed equally to this work.

0197-4580/$ – see front matter © 2019 Elsevier Inc. All rights reserved.
https://doi.org/10.1016/j.neurobiolaging.2019.08.006

Graham, 2002). In addition, this neurotransmitter is vulnerable to neurotoxic effects of various assemblies of Aβ (Esposito et al., 2013). With respect to synaptic transmission, the metabotropic glutamate receptor subtype 5 (mGluR5) is closely associated with AD pathology. Aβo induces mGluR5 clustering, which leads to an elevation in intracellular calcium (Renner et al., 2010). In addition, an mGluR5 antagonist reversed the learning and memory deficits observed in an animal model of AD (Um and Strittmatter, 2013).

To further understand the role of mGluR5 in AD, a study investigating the serial changes in Aβo-related neuropathogenesis of AD and assessing cognitive function is required. In the present study, we evaluate the changes in mGluR5 expression with disease progression in an AD mouse model via behavioral tests, molecular imaging, and histological immunoassay.

2. Materials and methods

2.1. Animals

The 5xFAD transgenic mice express 5 mutant human genes associated with AD, that is 3 amyloid precursor protein (APP) genes (APPswe, APPflo, and APPlon) and 2 presenilin 1 (PS1 and PSEN1) genes (PSEN1 M146L and PSEN1 L286V). 5xFAD mice were obtained from Jackson laboratories (stock no. 006554). The 5xFAD transgene-positive male mice were crossed with B6/SJL F1 hybrid female mice. B6/SJL F1 hybrids were used as an age-matched wild type (WT). Both WT and 5xFAD (n = 6 for imaging studies and n = 8 for immunostaining, total n = 14, female) mice had access to a normal diet and autoclaved water *ad libitum*; they were housed in a specific pathogen-free facility. The detailed study protocol is illustrated in Fig. 1.

All the mouse-related procedures were in accordance with the guidelines establish by the Institutional Animal Care and Use Committee of the Korea Institute of Radiological and Medical Sciences (IACUC permit number: KIRAMS2017-0014). The data reported herein are in compliance with ARRIVE (Animal Research: Reporting in Vivo Experiments) guidelines for reporting animal experiments.

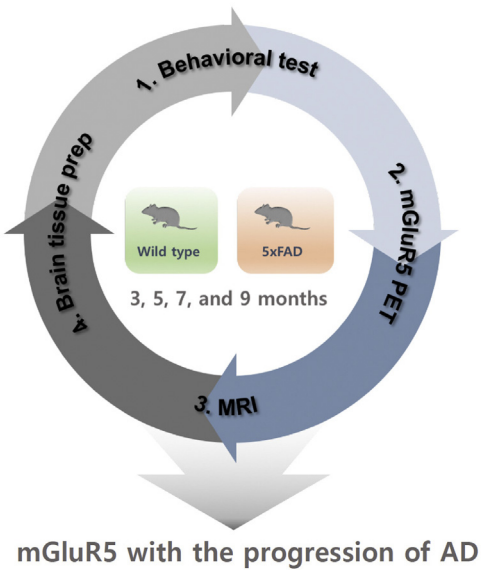

Fig. 1. Schematic protocol of the study. The behavioral tests and the imaging studies are separated from the histopathological immunoassay. Abbreviations: mGluR5, metabotropic glutamate receptor 5; AD, Alzheimer's disease; PET, positron emission tomography.

2.2. Behavioral tests

Mice (WT, n = 6; 5xFAD, n = 6, female) were subjected to both open fields and novel object recognition behavioral tests at 3, 5, 7, and 9 months of age. To ensure the animals' habituation to the experimenter, they were handled for 3 minutes on 7 consecutive days before the initiation of the investigation. At the beginning of each behavioral test, mice were adapted to the low-light illumination of the testing room for 30 minutes. The area surrounding the testing apparatus was cleaned with 70% ethanol between each experiment.

2.2.1. Open field test

The exploratory activity of mice in a novel environment was assessed during a 10-min test in an open field apparatus. The open field box comprised black acrylic walls (45 × 45 × 30 cm^3) and a central zone defined by a square-shaped area (22.5 cm × 22.5 cm). The mice were subjected to open field test at 3, 5, 7, and 9 months of age. Specifically, a single mouse was placed in the periphery of the field, and it was allowed to freely move for 10 minutes in the open field. The paths covered by the exploring animals were recorded using a video camera. Velocity (cm/s, average velocity), distance traveled (cm, total distance traveled), activity (%, mobility time over total time), ambulation (number of ambulations), and time in the center (s, time spent in the central zone) were determined through a tracking program (Viewer3, BIOSERVE GmbH, Mainz, Germany).

2.2.2. Novel object recognition memory test

The mice were subjected to the novel object recognition test to evaluate recognition memory at 3, 5, 7, and 9 months of age. The test was conducted for 3 consecutive days, after the open field test. On day 1, mice were acclimated to the testing box (width, 45 cm; length, 45 cm; height, 30 cm) devoid of objects for 10 minutes. By contrast, day 2 included a training session, in which 2 identical objects were placed 15 cm apart in the testing apparatus and the mice were allowed to explore them for 10 minutes. Finally, day 3 included a testing session, in which one of the objects was placed in the same location as it was during the training session while the other was replaced by a new differently shaped object (novel object). The animals were left to freely move in the object recognition testing box for 10 minutes. Mouse activity and exploratory behavior were recorded with a video tracking system during both training (day 2) and testing (day 3) sessions. The exploration time and number of visits to each object were measured using a video analysis program (Viewer3, BIOSERVE GmbH). When the head of a mouse was oriented within an angle of 50° and a distance of 4 cm from an object, recognition was defined on the basis of the duration and number of visits to each object. The proportions of duration (%) and visits (%) corresponding to novel object were calculated relative to those corresponding to total objects.

2.3. Preparation of a radiotracer

Considering that [^{18}F]FPEB is commonly used for the evaluation of mGluR5 integrity, it was prepared by nucleophilic substitution of F-18 in the nitro-FPEB precursor as described previously (Wang et al., 2007). The specific activity of [^{18}F]FPEB was greater than 80 GBq/μmol at the end of synthesis; its radiochemical purity was over 99%.

2.4. Positron emission tomography scans

Four days after carrying out the behavioral tests, positron emission tomography (PET) experiments were conducted on the

same mice (n = 6 for each group) using an animal-dedicated PET scanner (nanoScan, Mediso Medical Imaging Systems, Budapest, Hungary). The scanner has a peak absolute system sensitivity of >9% in an energy window of 250–750 keV, an axial field of view (FOV) of 28 cm, a transaxial FOV of 35–120 mm, and a transaxial resolution of 0.7 mm at 1 cm off center.

All the mice were anesthetized with 2.5% isoflurane in oxygen, and 11.1 ± 1.7 MBq of [^{18}F]FPEB was administrated via the tail vein. PET scan was performed for 90 minutes in the list mode. Thereafter, PET data were reconstructed in user-defined time frames (10 seconds × 6 frames, 30 seconds × 8 frames, 180 seconds × 5 frames, and 600 seconds × 7 frames) with voxel dimensions of 0.86 × 0.86 × 0.80 mm^3 using a 3-dimensional order-subset expectation maximization algorithm (4 iterations and 6 subsets). For attenuation correction, micro-CT imaging was conducted immediately after the PET scan using a 50 kVp X-ray voltage with 0.16 mAs.

2.5. Image analysis

A study specific brain template was constructed as described by Vállez Garcia et al. (Vallez Garcia et al., 2015). Subsequently, individual MR image was spatially normalized to MR-based mouse atlas (M.Mirrion MRI template, embedded in the PMOD software (version 3.4, PMOD Technologies Ltd, Switzerland). Normalized brain MR images were summed and subsequently, a Gaussian filter (FWHM = 0.8 mm) was applied to minimize the noise-induced bias. The study specific brain MR template was generated by brain masking. After mean PET images (4–26 frames) were obtained from the dynamic PET image, each mean PET image was coregistered to the individual MR image. Successively, this PET image was spatially normalized to the MR template. Finally, individual dynamic PET images corresponding to both groups were spatially normalized to the MR template and brain making was applied.

The cortex, hippocampus, striatum, and cerebellum were selected as volumes of interests (VOIs) on the MR template. The cerebellum was used as a reference region because this region presents a low concentration of mGluR5 (Shigemoto et al., 1993). The regional time–activity curves were acquired from the VOIs, and they were normalized in the units of the standardized uptake value, which is calculated as (MBq/mL in tissue)/(MBq of tracer injected/body weight). The regional nondisplaceable binding potential (BP_{ND}) was calculated as the distribution ratio −1 on the basis of noninvasive Logan's graphical analysis (Logan et al., 1990). Voxel-based parametric mapping was also utilized in the Logan's method. For each group, individual parametric maps were averaged. Subsequently, the mean PET image was coregistered to MR template to obtain PET-MR image.

2.6. Magnetic resonance imaging scans

Two days after conducting the PET scans, MRI scans were performed on the same mice to define the anatomical VOIs (n = 6 for each group). MRI data were obtained on a 31 cm horizontal-bore Agilent 9.4 T scanner (Agilent Technologies, Santa Clara, CA, USA) using a 2-channel array mouse head surface coil (Rapid Biomedical GmbH, Rimpar, Germany). The image parameters for the 3D T2 turbo spin echo sequence were as follows: repetition time (TR) = 2500 ms; echo time (TE) = 7.45 ms; FOV = 20 mm × 20 mm × 10 mm; matrix size = 128 × 128 × 64; voxel size = 0.156 μm × 0.156 μm × 0.156 μm; echo train length = 3; and scan time = 1 hour 54 m 50 seconds.

2.7. MR spectroscopy

Mice (n = 6 for each group) were anesthetized with 1%–2% isoflurane, and MR spectroscopy (MRS) was conducted at 3, 5, 7, and 9 months of age. The static field homogeneity was adjusted using the first- and second-order shims via manual shim. During experiments, a 72 mm inner diameter volume coil for RF transmission (Rapid) and 2-channel array mouse head surface coil (Rapid) for signal reception were used.

T2-weighted localizer images were obtained in the coronal, axial plane using a multislice turbo spin echo protocol (TR/TE_{eff} = 3500/10 ms, echo train length = 6, FOV = 20 mm × 20 mm, slice thickness = 0.8 mm, 2 averages, and image matrix = 128 × 128). Proton (^{1}H) MR spectroscopy of volumes of interest (1.2 × 1.5 × 2.0 mm^3) centered in the left dorsal hippocampus was performed. A water-suppressed point-resolved spectroscopy (PRESS) pulse sequence was used for measuring metabolite levels. The parameters for PRESS data acquisition were as follows: TR/TE = 5000/13.87 ms, number of averages = 256, sweep width = 5 kHz, and number of sampling points = 2048. Outer volume suppression was used, which was interleaved with water signal suppression using variable power RF pulses with optimized relaxation delays. A non–water-suppressed reference PRESS spectrum was also acquired (8 averages).

Spectral fitting analysis was performed using the LCModel software (version 6.3-1L). Cramer-Rao lower bounds, represented as percentage standard deviations of metabolite estimates (%SD), were obtained from the LCModel to determine the precision of the metabolite signal estimates. The experimentally observed spectrum of macromolecules and the simulated spectra of the following 12 metabolites were included in the basis set for the LCModel: alanine (Ala), aspartate (Asp), creatine (Cr), phosphocreatine (PCr), γ-aminobutyric acid (GABA), glucose (Glc), glutamine (Gln), glutamate (Glu), myo-inositol (mIns), lactate (Lac), N-acetylaspartate (NAA), and taurine (Taur). Quantification was carried out using the absolute metabolite concentration. The LCModel fitting was performed over the spectral range of 1.0 ppm–4.4 ppm.

2.8. Brain sample preparation

Two age-matched mice per group were sacrificed (n = 2 × 4, total n = 8 for each group). After imaging studies, 3 mice per group at 9 months of age were also included the immunostaining experiments (total n = 5 for each group). After sacrificed their hemibrains were extracted for histological and molecular analysis. For each mouse, one hemibrain was fixed in 4% paraformaldehyde/phosphate-buffered saline (PBS) for immunohistochemistry, whereas the other hemibrain was dissected and its hippocampus was immediately placed in ice as described previously (Hagihara et al., 2009); this hippocampus was subsequently stored at −80 °C for western blotting.

2.9. Western blotting

The hippocampus was homogenized with tissue lysate buffer (Pro-prepTM, Intron Inc, Gyeonggi-do, Korea). After sonication, the protein concentration of the total extract was measured via the Bradford assay (Bio-Rad, Hercules, CA, USA). Protein extract (10 μg) was resuspended in SDS (sodium dodecyl sulfate)-bromophenol blue reducing buffer with 250 mM Tris, 40% glycerol, 10% mercaptoethanol, and 4% SDS. Western blotting was performed using 10% SDS-polyacrylamide gel and a nitrocellulose membrane. The blots were blocked with 5% skim milk in 0.1% Tween-20 in PBS for 30 minutes and incubated overnight with rabbit anti-mGluR5 (1:5000, ab76316, Abcam, Cambridge, UK) or mouse anti-actin

antibody (1:5000; A1978, Sigma, St. Louis, MO, USA); they were then washed with 0.1% Tween-20 in PBS and incubated with secondary antibodies (biotinylated anti-rabbit or anti-goat). Immunoactivity was detected using an enhanced Western Lightning Plus-ECL (NEL104001EA, PerkinElmer, Inc, Waltham, MA, USA). Optical density of the detected bands was quantified using the NIH ImageJ software (imagej.nih.gov/ij/), and it was normalized by actin expression.

2.10. Immunohistochemistry

Formalin-fixed mouse brains were first cranially divided into the cortex and striatum region (from 0.84 mm to 1.34 mm at the bregma) and into the hippocampus and thalamus region (from −1.94 mm to −1.58 mm at the bregma) using disposable blades. They were then embedded into paraffin and sectioned into 3-μm thick slices. After dewaxing and rehydration, the sections were retrieved with antigen citrate buffer for 30 minutes; the endogenous peroxidase activity was blocked by incubating them with 0.3% H_2O_2 in absolute methanol for 15 minutes at room temperature (RT). After immunoperoxidase labeling, the sections were blocked in normal horse serum (S-200, Vector Laboratories, Burlingame, CA, USA) and incubated overnight at 4 °C in a humidity chamber with the primary antibody, mouse anti-6E10 (1:2000, SIG-39320, Covance, Princeton, NJ, USA). The next day, all the sections were washed with PBS-Triton X-100 (0.1%) buffer, allowed to react with each biotinylated secondary antibody for 30 minutes at RT, and then washed and incubated for 30 minutes at RT with an avidin–biotin peroxidase complex (PK-6100, Vector Laboratories) prepared according to the manufacturer's instructions. After washing with PBS-Triton X-100 buffer, the peroxidase reaction was initiated using a diaminobenzidine substrate (DAB, SK-4100, Vector Laboratories), which was also prepared according to the manufacturer's instructions. Counterstaining was conducted with hematoxylin for 30 seconds before mounting the sections. The images of the stained brain sections were captured using a BX-53 microscope equipped with a CCD DP73 digital camera (Olympus, Tokyo, Japan). The quantification of beta-amyloid plaques bigger than 10 μm^2 was carried out using the NIH ImageJ software (imagej.nih.gov/ij/). In addition, the number and size of plaques were determined in the hippocampus, cortex, striatum, and thalamus.

2.11. Statistical analysis

Except immunostaining experiments from 3 to 7 months of age, all the data are presented as mean ± standard deviation (SD) because 2 mice per time points were used in the immunostaining experiments. Behavioral test was analyzed using the two-way analysis of variance. Differences in BP_{ND} values and mGluR5 protein expression at 9 months of age were analyzed using the Mann–Whitney *U* test. Statistical significance was defined at a *p*-value lower than 0.05. All statistical analyses were performed using GraphPad Prism (GraphPad software, Inc, La Jolla, CA, USA).

3. Results

3.1. Behavioral tests

As shown in Fig. 2, general locomotor activity of the 5xFAD and WT mice at 3 and 5 months of age was similar. However, the distance traveled and velocity were observed to be higher in the 5xFAD group than in the WT group, starting from the age of 7 months. In addition, the 5xFAD mice showed higher retention in the center than WT mice did at this time point.

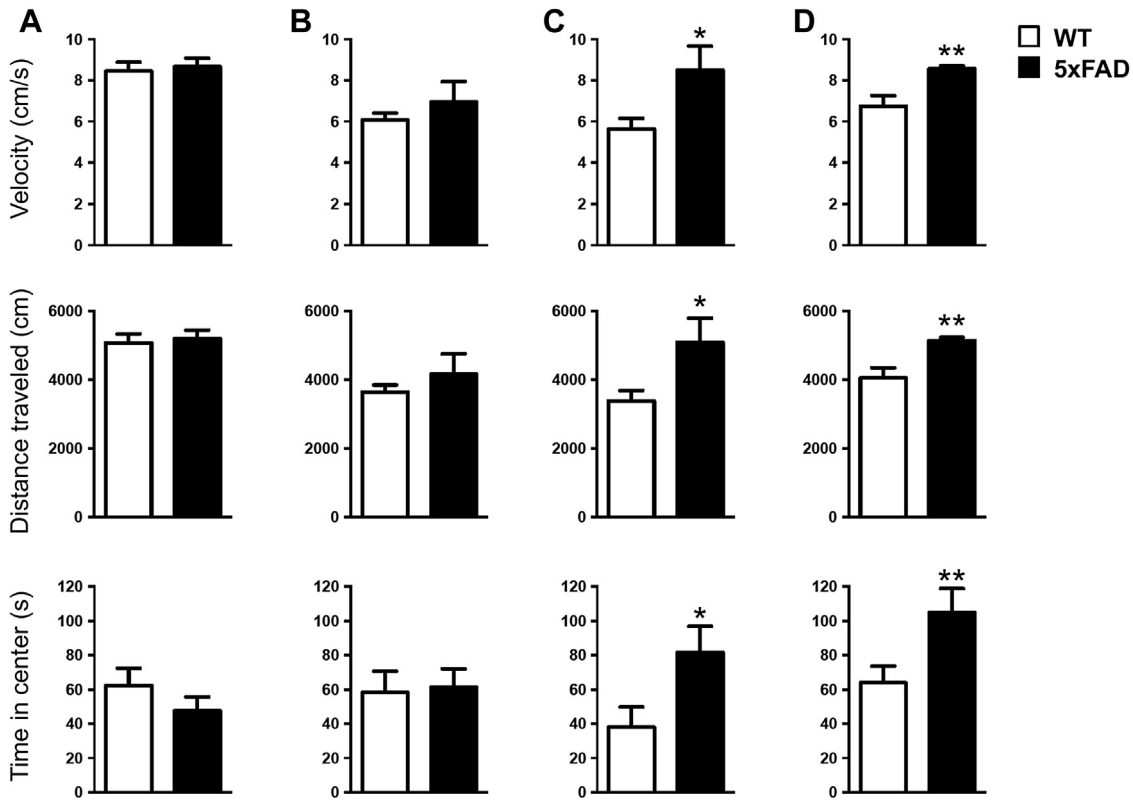

Fig. 2. The 5xFAD mice showed hyperactive and decreased anxiety-like behavior from the age of 7 months. Values are presented as mean ± standard deviation (n = 6). (A) 3 months, (B) 5 months, (C) 7 months, and (D) 9 months of age. Statistical significance was defined as $^{*}p < 0.05$, $^{**}p < 0.01$. Abbreviations: WT, wild type.

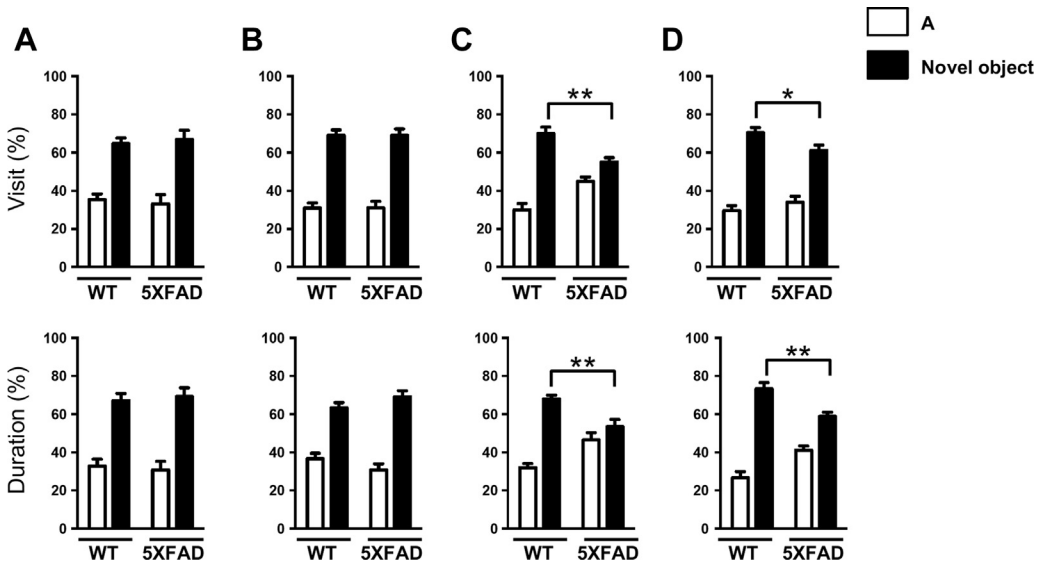

Fig. 3. The 5xFAD mice displayed memory dysfunction from 7 months of age. (A) 3 months, (B) 5 months, (C) 7 months, and (D) 9 months of age. Values are presented as mean ± standard deviation (n = 6). Statistical significance was defined as $^{*}p < 0.05$, $^{**}p < 0.01$. Abbreviations: WT, wild type.

To evaluate recognition memory in the 5xFAD mice, the object recognition memory test was performed at the ages of 3, 5, 7, and 9 months. No statistically significant difference in the preference for the novel object was observed between the WT and 5xFAD mice at 3 and 5 months of age. However, the 5xFAD mice showed lower preference to the novel object than the age matched WT mice did from 7 months of age (Fig. 3).

3.2. Longitudinal mGluR5 PET

In WT mice, no significant differences in brain uptake were observed over time. By contrast, the regional time-activity curves for the 5xFAD mice showed that radioactivity levels in mGluR5-rich regions (i.e., cortex, hippocampus, and striatum) changed according to the time point. Specifically, at 5 months of age, the brain uptake in the 5xFAD mice was reduced by 25%–29%; this was then increased by 21%–27% at 7 months of age to finally decrease by 24%–28% at 9 months of age. By contrast, cerebellar radioactivity levels remained constant at all ages.

In voxel-wise analysis, BP_{ND} values for the WT mice were similar over time, whereas those for the 5xFAD mice fluctuated. Specifically, BP_{ND} values observed at 5 months of age were 30%–31% lower than those observed at an earlier time point. In addition, the values at 7 months of age increased by 51%–61%, whereas

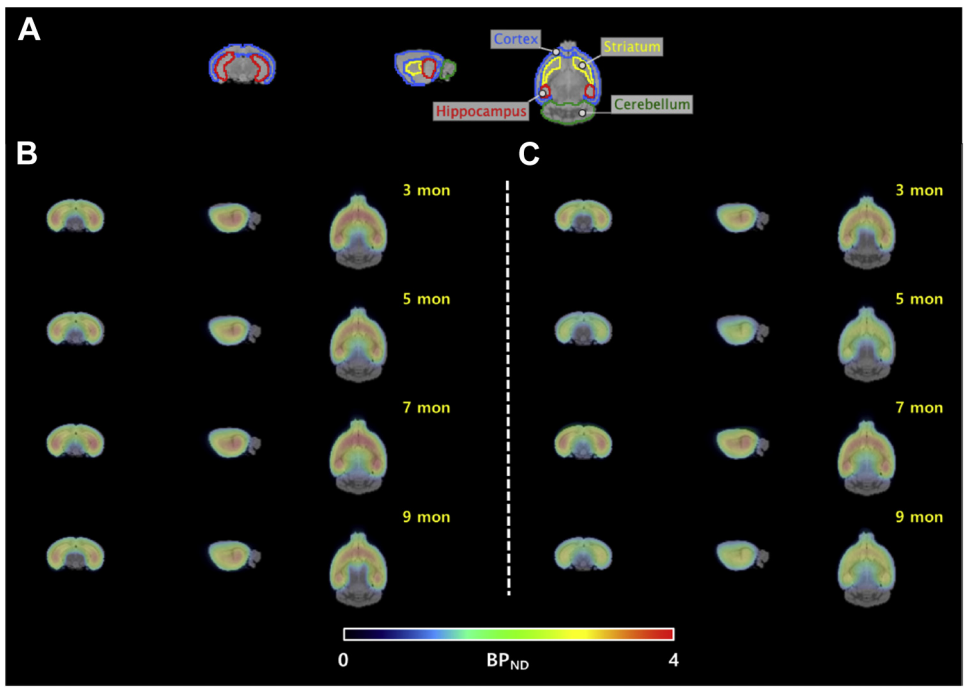

Fig. 4. Definition of volumes of interest (A) and comparison of the binding values for mGluR5 between the (B) WT and (C) 5xFAD mice. Abbreviations: WT, wild type.

Table 1
Binding values in the WT and 5xFAD mice

	3 mo	5 mo	7 mo	9 mo
Wild type				
Striatum	4.52 ± 0.68	4.31 ± 0.57	4.28 ± 0.62	4.16 ± 0.53
Hippocampus	4.17 ± 0.43	4.14 ± 0.59	4.12 ± 0.47	4.08 ± 0.50
Cortex	2.80 ± 0.51	2.40 ± 0.75	2.77 ± 0.52	2.80 ± 0.39
5xFAD				
Striatum	4.17 ± 0.65	2.93 ± 0.77	4.56 ± 0.91	2.88 ± 0.40[a]
Hippocampus	3.92 ± 0.58	2.75 ± 0.68	4.42 ± 0.88[a]	2.59 ± 0.53[a]
Cortex	2.64 ± 0.49	1.83 ± 0.43	2.84 ± 0.63	1.71 ± 0.24[a]

Data are presented as mean ± standard deviation.
Key: WT, wild type.
[a] $p < 0.05$ for the comparisons between months. n = 6.

the values at 9 months of age decreased by 37%–42% (Fig. 4, Table 1).

3.3. ^{1}H MRS analysis

The comparison of the neurochemical profiles of the left dorsal hippocampus between the 5xFAD and WT mice is shown in Fig. 5. At the age of 3 months, no statistically significant differences were observed, with the exception of Lac, which showed a significant decrease in the AD mouse model ($p = 0.019$). However, at 5 months of age, a decrease in Glu ($p = 0.003$), NAA ($p = 0.006$), and Taur ($p = 0.0001$) levels and an increase in Lac level were observed in the 5xFAD mice. At 7 months of age, the 5xFAD mice showed a significant decrease in Cr ($p = 0.002$), GABA ($p = 0.004$), and Taur ($p = 0.006$) levels and an increase in mIns ($p = 0.0009$) level. Furthermore, at 9 months of age, the level of Cr ($p = 0.048$) was observed to decrease, whereas those of PCr ($p = 0.037$) and mIns ($p = 0.020$) were observed to increase. Although no statistically significant differences were observed, the concentrations of Glu, GABA, and NAA were lower in the 5xFAD mice than in the WT mice (Figure S1 and S2).

3.4. Immunohistochemistry

In the 5xFAD mice, Aβ accumulation was observed throughout the brain; however, no pathologic findings were observed in WT mice. The most abundant site of Aβ accumulation in the 5xFAD mice was the hippocampus, followed by the thalamus, cortex, and striatum. The results of quantification revealed that Aβ accumulation increased with time (Fig. 6).

3.5. Quantification of mGluR5 protein level

In WT mice, mean mGluR5 protein levels did not significantly differ with time. In the 5xFAD mice, the expression levels of mGluR5 at 3 months of age were similar to that in WT. But the concentration decreased at 5 months of age in 5xFAD mice, to increase again at 7 months of age and finally further decrease at 9 months of age. At this age, the protein level for 5xFAD group statistically significant decreased compared with WT group (Fig. 7, $p = 0.0079$). Furthermore, the results of longitudinal PET study showed a similar trend.

4. Discussion

The present study aimed at evaluating the changes in mGluR5 in an animal model of AD with the progression of the disease. In particular, we examined the motor and cognitive function as well as the neurochemical change within individual mice. Furthermore, we

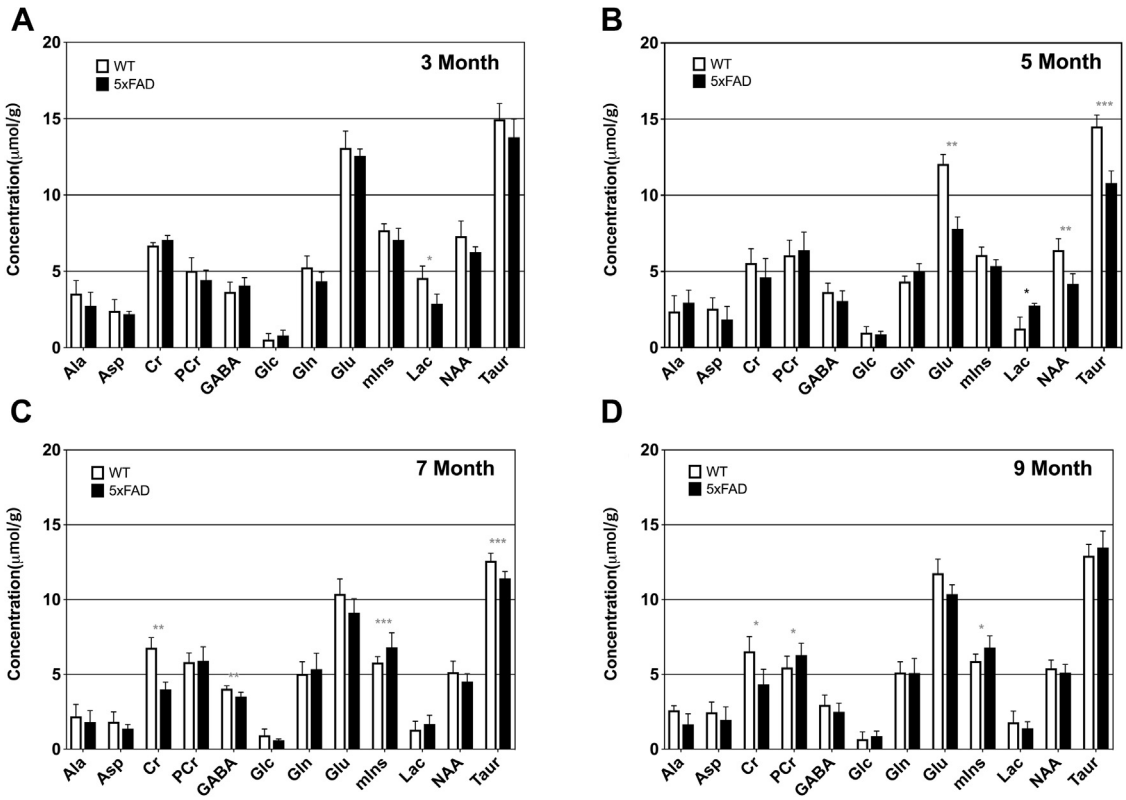

Fig. 5. Comparison of the neurochemical profiles between the WT and 5xFAD mice. (A) 3 months, (B) 5 month, (C) 7 months, and (D) 9 months of age. Values are presented as mean ± standard deviation (n = 6). Statistical significance was defined as $^*p < 0.05$, $^{**}p < 0.01$, and $^{***}p < 0.001$. Abbreviations: WT, wild type.

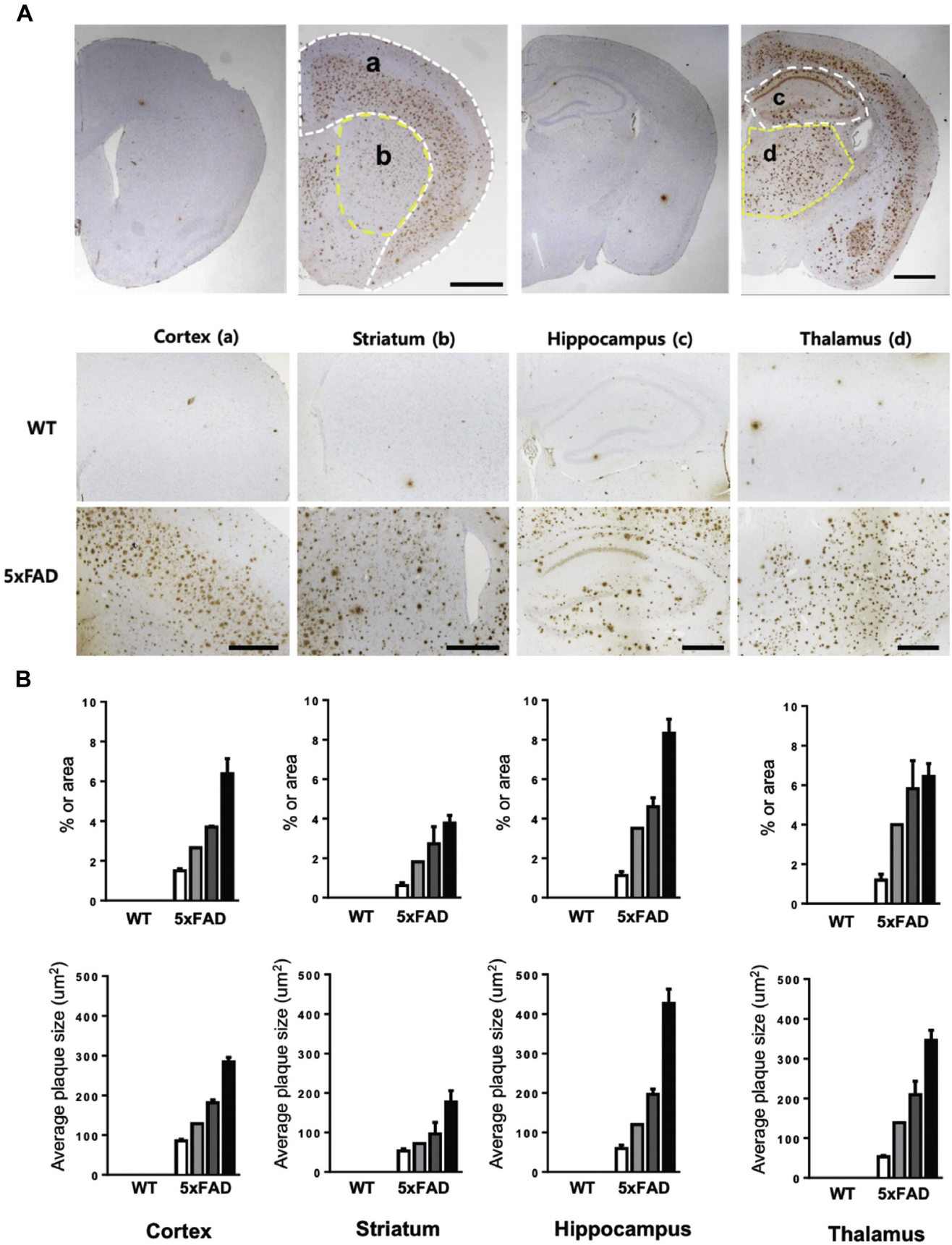

Fig. 6. Aβ pathological analysis between the WT and 5xFAD mice in the cortex, striatum, hippocampus, and thalamus. (A) Immunohistochemical staining of Aβ at 9 months of age; (B) quantification of Aβ deposition at 3, 5, 7, and 9 months of age. Values are presented as mean ± standard deviation (n = 2–6). Abbreviations: Aβ, amyloid β; WT, wild type.

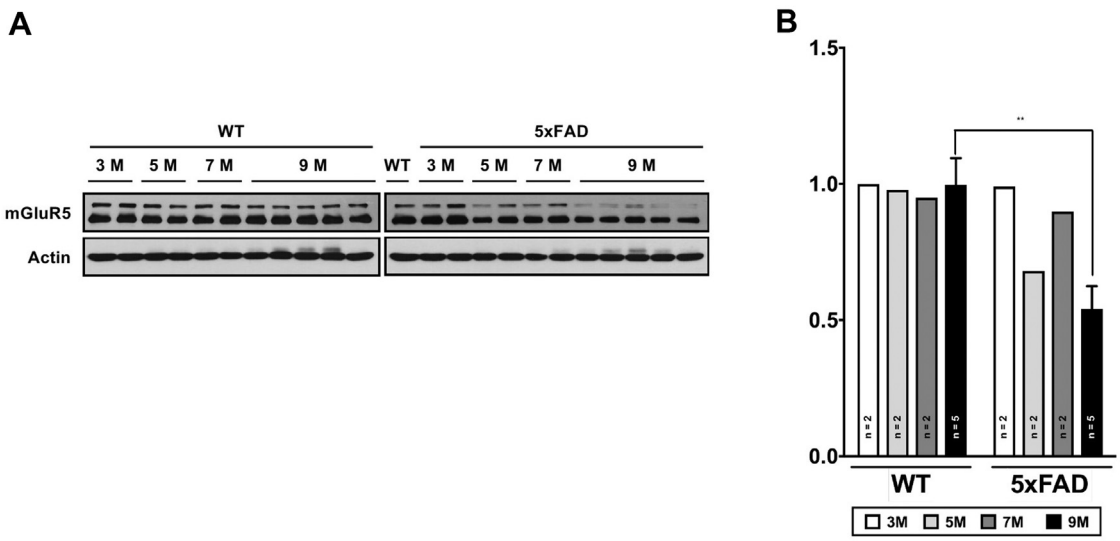

Fig. 7. Comparison of the protein expression of mGluR5 between the WT and 5xFAD mice (A). Values are presented as a mean value from 3 to 7 months of age (n = 2, respectively) and as mean ± standard deviation (n = 5, respectively) at 9 months of age (B). Statistical analysis for 9 months mGluR5 expression in the WT or 5xFAD mice was performed using Mann-Whitney *U* test. Statistical significance was defined as $^{**}p < 0.01$. Abbreviations: mGluR5, metabotropic glutamate receptor 5; WT, wild type.

validated the pathology in age-matched animals. In the behavioral tests, the 5xFAD mice displayed severe hyperactive behavior and decreased anxiety-like behavior as well as learning and memory deficit from the age of 7 months because memory-impaired mice have lower preference to the novel object than the previously encountered one. From a neuroimaging point of view, Aβ pathology induced alterations in the mGluR5 and neurochemical profiles. In addition, histopathology demonstrated that the protein expression of mGluR5 changes dynamically because of amyloid deposition. To the best of our knowledge, this is the first study that elucidated the serial changes in mGluR5 protein expression in the Aβo-related neuropathogenesis of AD.

The advantages of using molecular imaging technologies include the early detection of pathology and the assessment of therapeutic effects in a noninvasive manner. The progression of AD begins with a change at the molecular level; consequent functional and structural changes in turn cause clinical symptoms. To differentiate the functional changes, radiopharmaceuticals must have a high signal-to-noise ratio. Although many researchers attempted to differentiate AD in murine brains, in the past, most of the studies did not yield robust results. In amyloid and tau PET, the difference in specific binding of radiotracer between the AD and healthy animal groups is very minor. Poisnel et al. observed an increased uptake of radiotracer using amyloid PET in APP/PS1 mice at 5 months of age although further increase at 12 months of age was not observed; these results contrasted the histological findings (Poisnel et al., 2012). In addition, the binding value of [^{11}C]PIB to Aβ in Tg2576 mice was not significantly higher than that in WT mice (Toyama et al., 2005). With regard to tau PET, [^{18}F]THK5117 showed only 0.15–1.31 of the specific binding in the P301S mice (Brendel et al., 2016). Despite successful binding in humans, the radiotracers failed to show discrimination in AD mice; this is probably due to the difference in the morphology of plaques.

The changes in binding values of mGluR5 over time can be explained by the amyloid pathology and neuroinflammation. In the early state of AD, amyloid plaques directly influence the glutamate signaling and glial cells perform physiological roles without manifesting clinical symptoms. In the middle of the disease, however, amyloid pathology induces neuroinflammation by the overactivation of glial cells. Eventually, neurotoxic factors cause neuronal death and consequently, decrement of available receptors on the plasma membrane (Serrano-Pozo et al., 2011, 2016). From these perspectives, downregulation of mGluR5 without behavioral deficits at 5 months of age is the result of dominant amyloid pathology. This result is also validated by the observed decrease in mGluR5 protein level. Rupsingh et al. also reported a reduction in hippocampal glutamate, in patients with AD (Rupsingh et al., 2011). In the present study, MRS data also displayed a significant reduction in Glu, NAA, and Taur levels. The levels of Glu and NAA are reportedly related to neuronal integrity and the number of surviving neurons (Glodzik et al., 2015; Ramadan et al., 2013). The reduced taurine level is thought to be due to an imbalance in major neurochemicals (Kulak et al., 2010) and neurogenesis (Gebara et al., 2015). As AD progresses, amyloid pathology induces the overactivation of glia cells as well as an increment of intracellular Ca^{2+} concentration. These events accelerate the release of neurotoxins including proinflammatory cytokines, reactive oxygen species, and radicals. Recently, Herde et al. demonstrated that neuroinflammation leads upregulation of mGluR5 (Muller Herde et al., 2019). In the present study, mGluR5 PET showed mGluR5 upregulation and behavioral deficit at 7 months of age; this may be mainly due to neuroinflammatory process. Because mGluR5 is expressed in neurons as well as in the activated astrocytes and microglia (Byrnes et al., 2012; Ferraguti and Shigemoto, 2006). At this time point, MRS showed a decrease in GABA and Taur levels and an increase in mIns levels. These results imply a deficit in inhibitory functions and a decreased neurogenesis. mIns expression is high in glial cells; therefore, an increment in mIns level indicates the activation of glial cells. Finally, downregulation of mGluR5 at 9 months of age can be explained by the permanent neuronal loss caused by the cumulative effect of chronic inflammation. An increase in mIns level and a decrease in NAA and Glu levels represents the typically observed MRS pattern in AD studies (Lin et al., 2014; Ross et al., 1998). The patterns of upregulation and downregulation of the receptor are similar to those observed by Ikonomovic et al. (Ikonomovic et al., 2003), that is the cholinergic system shows a transient upregulation in subjects with mild cognitive impairment, followed by a depletion as AD progresses to the advanced stage.

The limitations of this study include low sample size and lack of inflammation-related experimental data that are comparable with

mGluR5 PET results. If additional experiments are carried out from the perspective of neuroinflammation with disease progression, we can improve our understanding of AD pathophysiology and possibly find an optimal time point for the initiation of therapeutic interventions before the occurrence of irreversible neuronal changes.

In conclusion, we demonstrated that mGluR5 PET successfully differentiates the severity of AD and further validated it using histopathology. Considering that the changes in mGluR5 binding occurred before behavioral perturbation, mGluR5 PET could serve as a sensitive in vivo imaging tool for the detection of AD.

Disclosure

The authors have no actual or potential conflicts of interest.

Acknowledgements

This research was supported by a grant of the National Research Foundation of Korea (Grant No. NRF-2017R1C1B5018250), INHA UNIVERSITY HOSPITAL Research Grant, and a grant from the Korea Institute of Radiological and Medical Sciences, funded by the Ministry of Science and ICT (MSIT), Republic of Korea (50536-2019).

Appendix A. Supplementary data

Supplementary data to this article can be found online at https://doi.org/10.1016/j.neurobiolaging.2019.08.006.

References

Allen, N.J., Barres, B.A., 2005. Signaling between glia and neurons: focus on synaptic plasticity. Curr. Opin. Neurobiol. 15, 542–548.
Alzheimer, A., Stelzmann, R.A., Schnitzlein, H.N., Murtagh, F.R., 1995. An English translation of Alzheimer's 1907 paper, "Uber eine eigenartige Erkankung der Hirnrinde". Clin. Anat. 8, 429–431.
Brendel, M., Jaworska, A., Probst, F., Overhoff, F., Korzhova, V., Lindner, S., Carlsen, J., Bartenstein, P., Harada, R., Kudo, Y., Haass, C., Van Leuven, F., Okamura, N., Herms, J., Rominger, A., 2016. Small-animal PET imaging of tau pathology with ^{18}F-THK5117 in 2 transgenic mouse models. J. Nucl. Med. 57, 792–798.
Byrnes, K.R., Loane, D.J., Stoica, B.A., Zhang, J., Faden, A.I., 2012. Delayed mGluR5 activation limits neuroinflammation and neurodegeneration after traumatic brain injury. J. Neuroinflammation 9, 43.
Esposito, Z., Belli, L., Toniolo, S., Sancesario, G., Bianconi, C., Martorana, A., 2013. Amyloid beta, glutamate, excitotoxicity in Alzheimer's disease: are we on the right track? CNS Neurosci. Ther. 19, 549–555.
Ferraguti, F., Shigemoto, R., 2006. Metabotropic glutamate receptors. Cell Tissue Res. 326, 483–504.
Fields, R.D., Stevens-Graham, B., 2002. New insights into neuron-glia communication. Science 298, 556–562.
Francis, P.T., Ramirez, M.J., Lai, M.K., 2010. Neurochemical basis for symptomatic treatment of Alzheimer's disease. Neuropharmacology 59, 221–229.
Gebara, E., Udry, F., Sultan, S., Toni, N., 2015. Taurine increases hippocampal neurogenesis in aging mice. Stem Cell Res. 14, 369–379.
Glodzik, L., Sollberger, M., Gass, A., Gokhale, A., Rusinek, H., Babb, J.S., Hirsch, J.G., Amann, M., Monsch, A.U., Gonen, O., 2015. Global N-acetylaspartate in normal subjects, mild cognitive impairment and Alzheimer's disease patients. J. Alzheimers Dis. 43, 939–947.
Grothe, M.J., Barthel, H., Sepulcre, J., Dyrba, M., Sabri, O., Teipel, S.J., Alzheimer's Disease Neuroimaging, I., 2017. In vivo staging of regional amyloid deposition. Neurology 89, 2031–2038.
Hagihara, H., Toyama, K., Yamasaki, N., Miyakawa, T., 2009. Dissection of hippocampal dentate gyrus from adult mouse. J. Vis. Exp. 1543.
Ikonomovic, M.D., Mufson, E.J., Wuu, J., Cochran, E.J., Bennett, D.A., DeKosky, S.T., 2003. Cholinergic plasticity in hippocampus of individuals with mild cognitive impairment: correlation with Alzheimer's neuropathology. J. Alzheimers Dis. 5, 39–48.
Kulak, A., Duarte, J.M., Do, K.Q., Gruetter, R., 2010. Neurochemical profile of the developing mouse cortex determined by in vivo ^{1}H NMR spectroscopy at 14.1 T and the effect of recurrent anaesthesia. J. Neurochem. 115, 1466–1477.
Larson, E.B., Kukull, W.A., Katzman, R.L., 1992. Cognitive impairment: dementia and Alzheimer's disease. Annu. Rev. Public Health 13, 431–449.
Lin, Y., Yao, J., Chen, Y., Pang, L., Li, H., Cao, Z., You, K., Dai, H., Wu, R., 2014. Hippocampal neurochemical changes in senescent mice induced with chronic injection of D-galactose and NaNO(2): an in vitro high-resolution NMR spectroscopy study at 9.4T. PLoS One 9, e88562.
Logan, J., Fowler, J.S., Volkow, N.D., Wolf, A.P., Dewey, S.L., Schlyer, D.J., MacGregor, R.R., Hitzemann, R., Bendriem, B., Gatley, S.J., Christman, D.R., 1990. Graphical analysis of reversible radioligand binding from time-activity measurements applied to [N-^{11}C-methyl]-(-)-cocaine PET studies in human subjects. J. Cereb. Blood Flow Metab. 10, 740–747.
Muller Herde, A., Schibli, R., Weber, M., Ametamey, S.M., 2019. Metabotropic glutamate receptor subtype 5 is altered in LPS-induced murine neuroinflammation model and in the brains of AD and ALS patients. Eur. J. Nucl. Med. Mol. Imaging 46, 407–420.
Poisnel, G., Dhilly, M., Moustie, O., Delamare, J., Abbas, A., Guilloteau, D., Barre, L., 2012. PET imaging with [^{18}F]AV-45 in an APP/PS1-21 murine model of amyloid plaque deposition. Neurobiol. Aging 33, 2561–2571.
Ramadan, S., Lin, A., Stanwell, P., 2013. Glutamate and glutamine: a review of in vivo MRS in the human brain. NMR Biomed. 26, 1630–1646.
Reilly, J.F., Games, D., Rydel, R.E., Freedman, S., Schenk, D., Young, W.G., Morrison, J.H., Bloom, F.E., 2003. Amyloid deposition in the hippocampus and entorhinal cortex: quantitative analysis of a transgenic mouse model. Proc. Natl. Acad. Sci. U. S. A. 100, 4837–4842.
Reinikainen, K.J., Soininen, H., Riekkinen, P.J., 1990. Neurotransmitter changes in Alzheimer's disease: implications to diagnostics and therapy. J. Neurosci. Res. 27, 576–586.
Renner, M., Lacor, P.N., Velasco, P.T., Xu, J., Contractor, A., Klein, W.L., Triller, A., 2010. Deleterious effects of amyloid beta oligomers acting as an extracellular scaffold for mGluR5. Neuron 66, 739–754.
Ross, B.D., Bluml, S., Cowan, R., Danielsen, E., Farrow, N., Tan, J., 1998. In vivo MR spectroscopy of human dementia. Neuroimaging Clin. N. Am. 8, 809–822.
Rupsingh, R., Borrie, M., Smith, M., Wells, J.L., Bartha, R., 2011. Reduced hippocampal glutamate in Alzheimer disease. Neurobiol. Aging 32, 802–810.
Serrano-Pozo, A., Betensky, R.A., Frosch, M.P., Hyman, B.T., 2016. Plaque-associated local toxicity increases over the clinical course of Alzheimer disease. Am. J. Pathol. 186, 375–384.
Serrano-Pozo, A., Mielke, M.L., Gomez-Isla, T., Betensky, R.A., Growdon, J.H., Frosch, M.P., Hyman, B.T., 2011. Reactive glia not only associates with plaques but also parallels tangles in Alzheimer's disease. Am. J. Pathol. 179, 1373–1384.
Shigemoto, R., Nomura, S., Ohishi, H., Sugihara, H., Nakanishi, S., Mizuno, N., 1993. Immunohistochemical localization of a metabotropic glutamate receptor, mGluR5, in the rat brain. Neurosci. Lett. 163, 53–57.
Toyama, H., Ye, D., Ichise, M., Liow, J.S., Cai, L., Jacobowitz, D., Musachio, J.L., Hong, J., Crescenzo, M., Tipre, D., Lu, J.Q., Zoghbi, S., Vines, D.C., Seidel, J., Katada, K., Green, M.V., Pike, V.W., Cohen, R.M., Innis, R.B., 2005. PET imaging of brain with the β-amyloid probe, [^{11}C]6-OH-BTA-1, in a transgenic mouse model of Alzheimer's disease. Eur. J. Nucl. Med. Mol. Imaging 32, 593–600.
Um, J.W., Strittmatter, S.M., 2013. Amyloid-β induced signaling by cellular prion protein and Fyn kinase in Alzheimer disease. Prion 7, 37–41.
Vallez Garcia, D., Casteels, C., Schwarz, A.J., Dierckx, R.A., Koole, M., Doorduin, J., 2015. A standardized method for the construction of tracer specific PET and SPECT rat brain templates: validation and implementation of a toolbox. PLoS One 10, e0122363.
Wang, J.Q., Tueckmantel, W., Zhu, A., Pellegrino, D., Brownell, A.L., 2007. Synthesis and preliminary biological evaluation of 3-[^{18}F]fluoro-5-(2-pyridinylethynyl) benzonitrile as a PET radiotracer for imaging metabotropic glutamate receptor subtype 5. Synapse 61, 951–961.
Xu, Y., Yan, J., Zhou, P., Li, J., Gao, H., Xia, Y., Wang, Q., 2012. Neurotransmitter receptors and cognitive dysfunction in Alzheimer's disease and Parkinson's disease. Prog. Neurobiol. 97, 1–13.